Tunable phase structure in $NaNbO_3$ ceramics by grain-size effect, electric field and heat treatment

He Qi,[ab] Ge Wang[c], Yongcheng Zhang[d], Dawei Wang[e], Hui Liu,[b] Shiqing Deng,[b]

Ruzhong Zuo*[f] and Jun Chen*[ag]

a. Beijing Advanced Innovation Center for Materials Genome Engineering, Department of Physical Chemistry, University of Science and Technology Beijing, Beijing 100083, P. R. China.

b. School of Mathematics and Physics, University of Science and Technology Beijing, Beijing 100083, P. R. China.

c. Department of Materials, University of Manchester, Manchester S13 9PL, UK.

d. College of Physics, Center for Marine Observation and Communications, and National Demonstration Center for Experimental Applied Physics, Qingdao University, Qingdao, 266071, P. R. China.

e. Shenzhen Institute of Advanced Electronic Materials, Shenzhen Institute of Advanced Technology, Chinese Academy of Sciences, Shenzhen 518055, P. R. China.

f. Center for Advanced Ceramics, School of Materials Science and Engineering, Anhui Polytechnic University, Wuhu, 241000 P. R. China.

g. Hainan University, Haikou 570228, Hainan Province, China.

*Corresponding authors: E-mail: zuoruzhong@ahpu.edu.cn (R.Z. Zuo) junchen@ustb.edu.cn (J. Chen)

H. Qi, G. Wang and Y.C. Zhang contributed equally to this work.

Abstract:

Large polarization and strain change during antiferroelectric - ferroelectric phase transition under electric field is the foundation for realizing excellent electrical properties in antiferroelectric ceramics, therefore, the adjustment of antiferroelectricity and clarification of the corresponding mechanism is the foundation for controlling electrical properties. $NaNbO_3$ is the most complex perovskite system showing multiple antiferroelectric phases in a wide temperature range, in which the antiferroelectricity shows obvious instability with changing external and internal conditions, namely the antiferroelectric phase can be adjusted by grain-size effect, electric field and heat treatment. According to the systematical study in terms of the Rietveld refinement of synchrotron XRD and Raman, $NaNbO_3$ exhibits a ferrielectric $P2_1ma$ structure at room temperature, the ferroelectric component of which increases with decreasing grain size. Two antiferroelectric tetragonal phases exist around *Curie* temperature T_C before the entrance of antiferroelectric R phase zone, while an antiferroelectric monoclinic phase, which can be maintained to room temperature by annealing treatment, acts as the bridge for the depolarization of the poled $NaNbO_3$ with ferroelectric Q phase. A detailed phase diagram mainly focused on the antiferroelectric phase zones of $NaNbO_3$ is plotted, which gives a clear understanding about the polymorphic phase transitions under different conditions. The results concluded in this work would give a clear guidance for designing high-performance $NaNbO_3$-based lead-free ceramics from the point of structure.

1. Introduction

Based on the miraculous structure with antiparallel arrangement of cation displacements in neighboring unit cells, antiferroelectrics (AFEs) exhibit zero spontaneous polarization macroscopically [1-3]. As a result, large polarization change and volume expansion can be achieved during electric field induced AFE-ferroelectric (FE) phase transition, providing the foundation for realizing excellent energy storage properties, large electrostrains and et al. [4-8] $PbZrO_3$ is the first reported AFE material with antiparallel displacement of Pb cations and a four-layer periodicity of pseudocubic $(110)_c$ planes, yet typical feature of double polarization-electric field (*P*-*E*) hysteresis loops is hard to be detected owing to a lower driven field (E_{AF}) for AFE-FE phase transition than that of the dielectric breakdown strength. The value of E_{AF} and even the reversibility of AFE-FE phase transition could be modified by compositional modification, leading to the generation of excellent electrical performances in $PbZrO_3$-based AFE ceramics [3-6]. Moreover, many interesting polarization configurations have been designed in $PbZrO_3$-based AFEs, such as such as incommensurate antiferroelectric structure, imbalance sine-wave polarization configuration, multiple phase transition under electric field and on heating, making them to be flexible and tunable for applying in various conditions [9-12]. As the increased attention on environment protection, increased focus has been attracted on lead free AFEs in recent years.

$NaNbO_3$ (NN) is one of the most widely studied lead-free AFEs with complex phase structure evolution on heating [13,14]. After modification of antiferroelectricity and dielectric relaxation behavior, excellent energy storage properties and electrostrain behavior have been reported in NN-based lead-free AFEs [7,15-20]. However, there is still a lot of controversy

about the room temperature AFE phase structure and the mechanism for the adjustment of antiferroelectricity in NN-based ceramics [13,21-25]. It seems to be no doubt that the room-temperature AFE phase of NN is comprised of a commensurate modulation with a four-layer periodicity of basic perovskite cells along *b* axis, which has been widely confirmed by the detected 1/4 type superlattice in X-ray diffraction (XRD) and selected area electron diffraction patterns [15-18,23]. The room-temperature AFE phase of NN is most widely identified as P phase (*Pbma* space group) composed of $\sqrt{2}\times4\times\sqrt{2}$ supercell of the basic perovskite cell as well as $a^-b^+a^-/a^-b^-a^-$ complex oxygen octahedral tilting system [13]. Nb in each octahedron is displaced from the geometrical center to a direction lying almost exactly in the plane of the O3/O4 square. Na1 cations are essentially undisturbed while Na2 cations are off-center displaced antiparallelly [14]. The Neutron pair distribution function analysis indicated that the off-center displacement of Nb and Na are 0.15 Å and 0.4 Å, respectively [22]. According to the first principles calculations, the AFE P phase have a remarkably small energy difference from the polar Q phase ($P2_1ma$ space group) [16]. The small energy difference between these phases leads to the coexistence of AFE and FE phases at room temperature and the irreversible AFE-FE phase transition under electric field. The decreased tolerance and B-site polarizability after substituting of another ABO_3 were thought to be important factors for realizing reversible AFE-FE phase transition behavior in NN-based ceramics by some researchers [16-18], yet some contrary conclusions were also reported recently [20,26].

Besides the chemical regulation, antiferroelectricity can also usually be affected by external field, such as stress (including size effect), electric field and temperature. For

example, monotonously decreased E_{AF} have been found in pure $PbZrO_3$ on heating, resulting in signature double *P-E* loops close to *Curie* temperature T_C [27]. Enhanced ferroelectricity can commonly be found in AFEs with decreasing size (grain size and film thickness) [28-31]. In this work, influence of size effect, temperature, electric field and heat treatment on the antiferroelectricity of pure NN ceramic was systematically studied, which would provide a guidance for deeply understand the underly mechanism for the modification of antiferroelectricity in NN.

2. Experimental procedure

The NN ceramics were fabricated by a solid-state method using Na_2CO_3 (≥99.5%) and Nb_2O_5 (≥99.5%) (Sinopharm Chemical Reagent Co., Ltd., CN) as the starting materials. The NN powder was first synthesized through calcination at 800 ºC for 5 h, and then the as-synthesized NN powders were high-energy ball milled at 700 rpm together with 0.5 wt.% PVB binder for 12 h. The sample discs were sintered by conventional sintering and hot-press sintering at various temperatures for 2 h. According to the average grain size of 5 μm, 2 μm and 0.8 μm, the NN samples were marked as G5, G2 and G0.8, respectively. The ceramic samples were well polished, painted with silver paste and then fired at 550 ºC for 30 min. Several G5 samples was poled under 10 kV/mm at room temperature for 5 min, the poled samples are called as PG5. Several PG5 samples were annealed at 320 ºC for 10 min, the annealed samples are called as PG5A.

The grain morphology was characterized using a scanning electron microscope (SEM, S4800, HITACHI). Temperature and frequency dependent dielectric properties were measured

by an LCR meter (Agilent E4980A, Santa Clara, CA). A ferroelectric test system (Precision multiferroelectric; Radiant Technologies Inc, Albuquerque, New Mexico) with an accessory laser interferometer vibrometer (AE SP-S 120E, SIOS Mebtechnik, GmbH, Ilmenau, Germany) was used to measure the *P-E* hysteresis loops and *S-E* curves. In order to achieve *P-E* loops at high temperature, a high-temperature probing stage (HFS600E-PB2, Linkam Scientific Instruments, Tadworth, UK) was used. Temperature dependent X-ray diffraction (XRD) measurements were performed with Cu $K\alpha$ radiation at an acceleration condition of 40 kV and 30 mA (D/Max2500V; Rigaku, Tokyo, Japan). Synchrotron XRD (SXRD) measurements were performed at was carried out at 11-ID-C beamline (105.9 keV, λ = 0.1173 Å) of the Advanced Photon Source (APS) at Argonne National Laboratory and Spring-8 (λ=0.66 Å). In order to get diffraction data, the as-sintered ceramics were fractured into powders with about dozens of microns. Rietveld refinements were performed by using the program GSAS II. Raman spectra were collected at room temperature on well-polished pellets using 532 nm excitation using a Raman spectrometer (LabRam HR Evolution, HORIBA JOBIN YVON, Longjumeau Cedex, France).

3. Results

The grain morphology of NN ceramics sintered at different conditions are shown in Fig. 1. The pressureless sintered NN sample exhibits relatively high density over 97% as well as large average grain size about 5 μm, which is marked as G5. Hot press sintered samples exhibit relatively low relatively density of ~92% owing to the much lower sintering temperature, which are marked as G2 and G0.8, respectively.

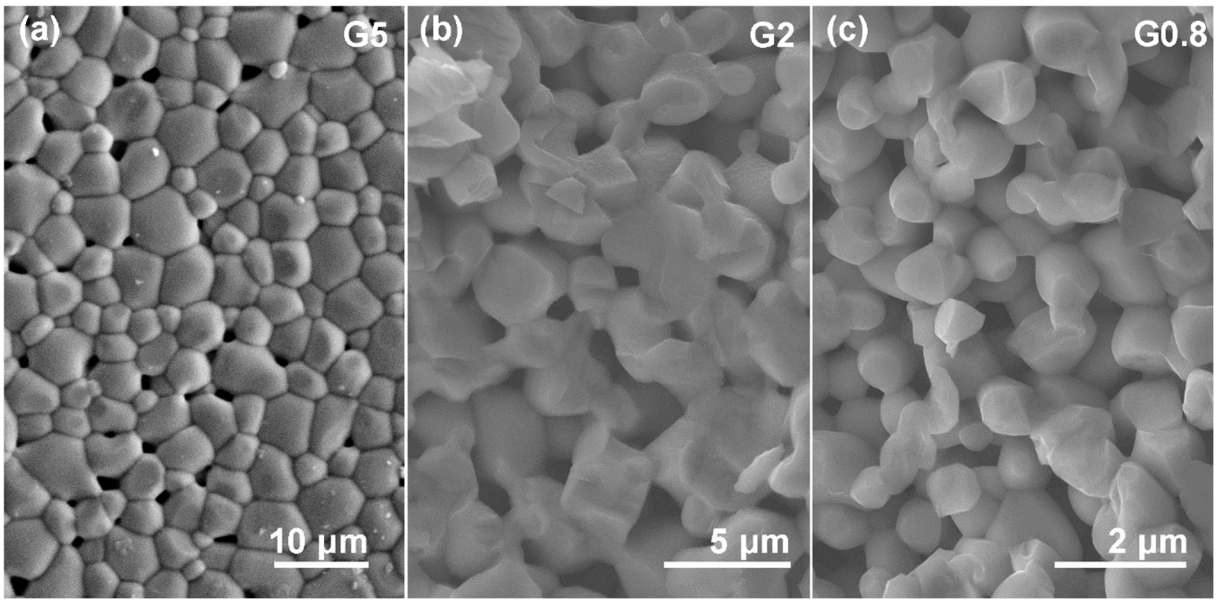

Fig. 1. SEM graphs of NN ceramics sintered at different conditions for 2 hours. The samples sintered by using (a) conventional sintering at 1370 ºC, (b) hot pressing sintering at 1250 ºC and (c) hot pressing sintering at 1100 ºC were named as G5, G2 and G0.8, respectively, according to the average grain size.

Temperature dependent dielectric permittivity at various frequencies of NN ceramics with different grain size are displayed in Fig. 2a, showing obviously complex polymorphic phase transition behavior on heating. Seven phases relating to N, P, R, S, T_1, T_2 and U have been widely reported in previous researches, the corresponding dielectric anomaly can also be found on the dielectric spectra, as marked in Fig. 2a. Interestingly, several additional dielectric anomalies can be seen at the same time: a weak relaxor peak at T_f~150 ºC for all unpoled samples, a weak anomaly at T_b~410 ºC for G5 sample, and a sharp increase of dielectric permittivity at T_a~320 ºC for G2 and G0.8 samples. For the NN sample poled at room temperature (PG5 in Fig. 2b), which is widely considered to be an FE Q phase, the relaxed dielectric anomaly at T_f~150 ºC cannot be detected, indicating that it should be related to the antiferroelectricity part in NN. A new dielectric anomaly at T_d~290 ºC should be related

to the depolarization of FE phase, because the successive dielectric peak at T_C~370 ºC still shows similar AFE phase transition feature to that of unpoled samples. This can be further confirmed by the repeatable double *P-E* loops in the temperature range of 290-370 ºC, as shown in Fig. 3. However, the AFE phase in the temperature range of 290-370 ºC should be different to that of G5 sample, this can be directly reflected by the missed T_f peak on the dielectric spectra of PG5A sample. These results indicate that the antiferroelectricity of NN ceramic can be easily modified by external process including size effect (preparation process), poling process and heat treatment, which needs a systematic study to reveal the detailed structure evolution.

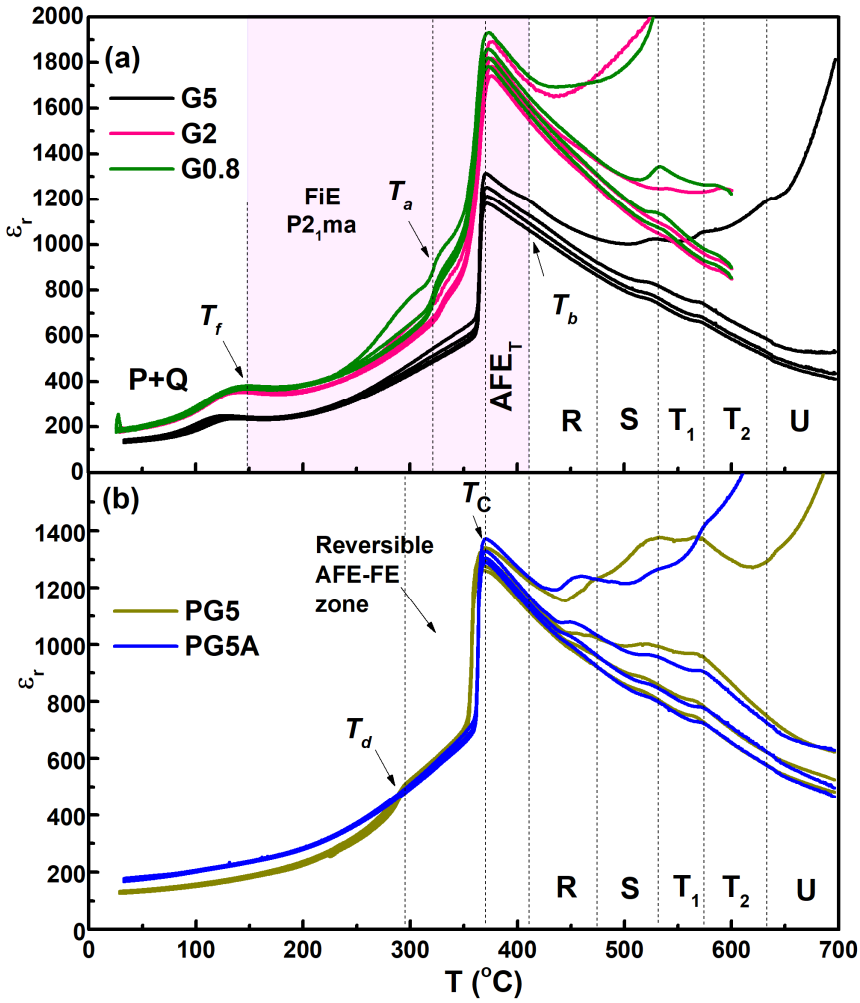

Fig. 2. Temperature and frequency dependent dielectric permittivity for different NN ceramics.

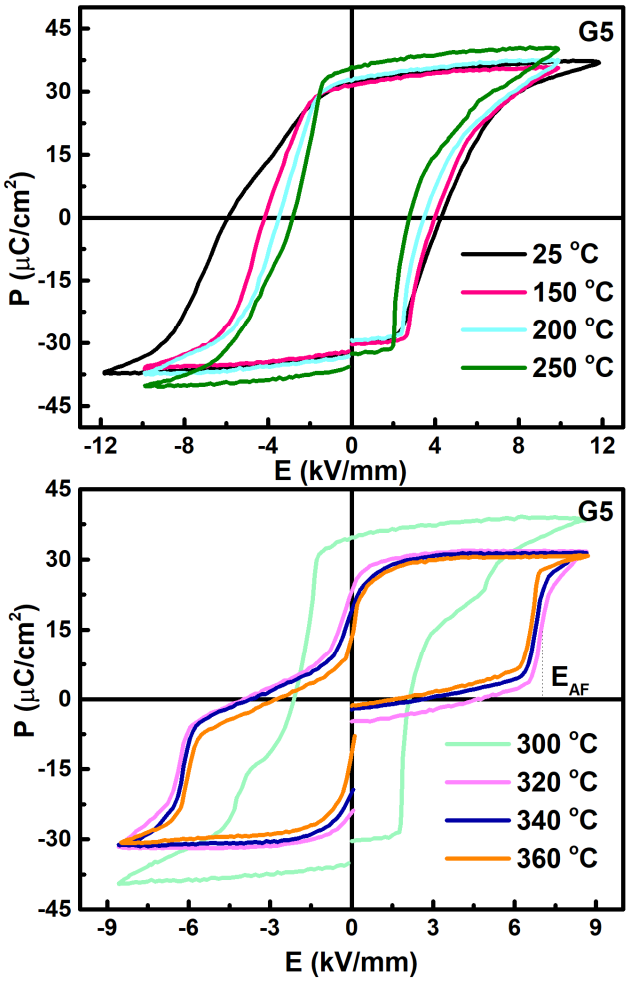

Fig. 3. Temperature dependent *P-E* loops of G5 sample.

4. Discussion

4.1 Size effect on antiferroelectricity

There are several different orthorhombic phases reported in NN ceramic, the most typical feature for distinguishing these phases is the superlattice diffractions [13-15,32]. According to the systematic studies by *Glazer* et al., antiphase and inphase oxygen octahedron tilt would lead to *(ooo)*/2 and *(ooe)*/2 types superlattice diffractions [33], respectively. For antiferroelectrics with commensurate and incommensurate structures, 1/*n* (*n* usually ≥3) type superlattice diffractions would also be detected depending on the

periodic polarization configuration [2,32]. It is well accepted that the AFE P and AFE R phases exhibit four-fold periodic supercell along *b* axis and six-fold periodic supercell along *c* axis, respectively, while FE Q phase only shows antiphase and inphase tilt along different axes. Therefore, the AFE P and AFE R phase can be identified by the characteristic 1/4 and 1/6 (or 1/3) type superlattice diffractions respectively from FE Q phase with only 1/2 type superlattice diffractions. However, it is quite hard to segregate FE Q from the matrix of AFE P phase, because FE Q phase not only shows the same symmetry but also constitutes by part of [BO_6] tilt features of AFE P phase. Namely, the AFE P phase can be considered as a "twinning" operation when compared with FE Q phase along *b* axis [25]. At the same time, owing to the poor resolution of X-ray diffraction for oxygen positions, the [BO_6] tilt information can be analyzed qualitatively instead of quantitatively, which is still enough to distinguish the various phases in NN-based ceramics.

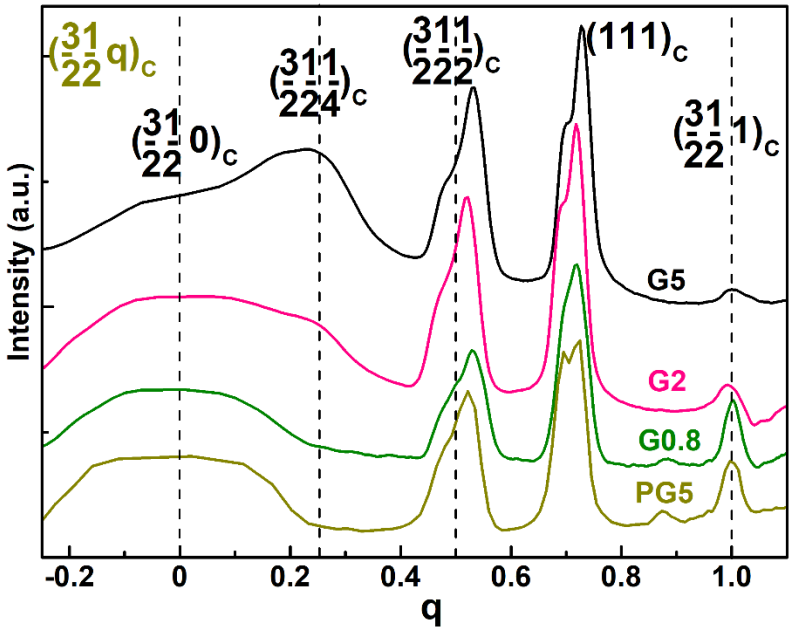

Fig. 4. *(3/2 1/2 q)$_C$* diffraction peaks for various NN ceramics at room temperature.

The high-energy SXRD for various NN samples were measured in order to analyze the structure evolution. In order to show the evolution of diffraction peaks between different structures more clearly, $(hkl)_C$ indices based on cubic perovskite cell are used in the paper. Equivalence indices for supercells can be transformed by using the method given in Fig. S1. The room temperature $(3/2\ 1/2\ q)_C$ diffraction peaks are shown in Fig. 4. With decreasing grain size, the intensity of q=1/4 peak decreases monotonously, suggesting the weakening of antiferroelectricity. A pure FE Q phase can be identified for the PG5 sample. It can be clearly shown in Fig. 4 (transformed from Fig. S2) that the AFE P dominated G5 sample also exhibits various half type superlattice diffractions similar to FE Q phase, thus the existence of FE Q phase in AFE dominated phase is hard be estimated through the existence of half type diffractions. In order to show the structure evolution more clearly, Rietveld refinement was taken and the results are shown in Fig. 5. The previous studies usually thought that the coexistence of antiferroelectricity and ferroelectricity in NN ceramics should be the coexistence of AFE P and FE Q phase, moreover, the relative fractions of the P and Q phases might be adjusted by the volume of twin boundary regions with respect to the twin variants [25]. The proposal of coexistence of AFE and FE Q phase by previous researchers is owing to the similar free energy of these two phases at room temperature [16]. However, this phase zone appears at T_C~370 ^oC during cooling, slightly below which obvious difference of free energy between AFE and FE phases can be supposed by the repeatable double *P-E* loops (Fig. 3). Namely, it is not easy to form the AFE-FE coexisted phase during cooling across T_C. Moreover, the reciprocal-space diffraction data is suitable for revealing the long-range average structure

instead of local structure information, and no direct evidence can be given to support the "twin structure" model recently. Therefore, even though the unpoled samples can be well identified by the coexistence of AFE P and FE Q phases with low reliability factors of weighted patterns (R_w) values in Figs. 5a-c, a single ferrielectric (FiE) phase is also used for Rietveld refinement. It can be found that the fit between the observed and calculated profiles is also satisfactory for all the studied ceramics by using an FiE phase, which shows similar low R_w values to that of AFE-FE coexisted phase. As a result, the room temperature structure of NN ceramics should be more suitable by using an FiE phase, which exhibits $P2_1ma$ space group and unbalanced antiparallel displacement of Nb cations with q=1/4. In order to solve the insufficient resolution of XRD for oxygen position, neutron powder diffraction of G5 sample was measured as a case study. Rietveld refinements were taken by using different space groups [24], as shown in Fig. S3. According to the most satisfied result by using an FiE $P2_1ma$ structure, structural parameters, fractional atomic coordinates, and equivalent isotropic displacement parameters are listed in Table S1.

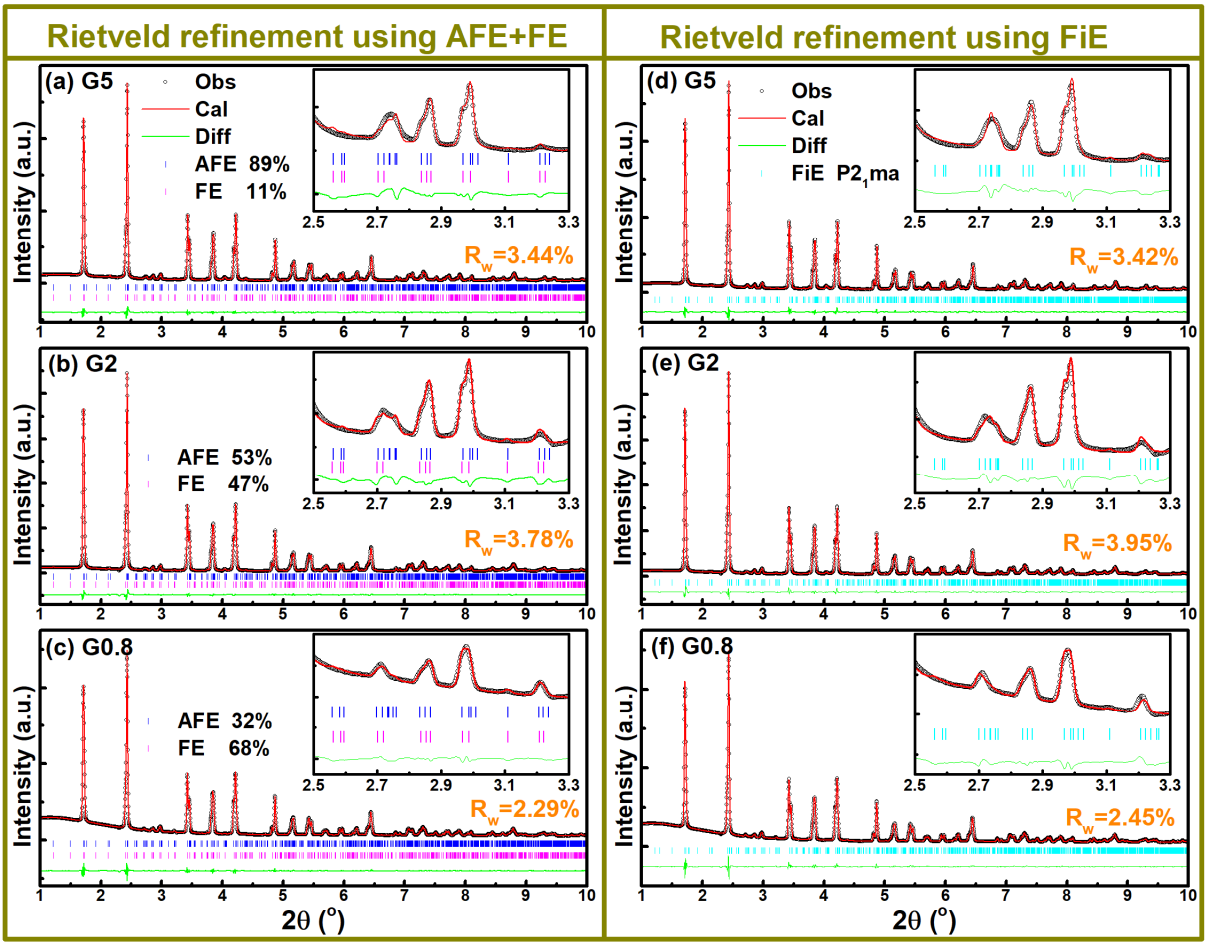

Fig. 5. Rietveld refinement results of room-temperature high-energy SXRD (λ=0.1173 Å) for various NN ceramics.

4.2 Electric field induced phase transition

Even though the antiparallel displacement feature can be eliminated, the orthorhombic symmetry with cation displacement toward the $[110]_C$ directions and $a^-b^+c^-$ oxygen octahedron tilt remains after poling under strong electric field, relating to FE Q phase. This can be well confirmed by the satisfactory Rietveld refinement result of PG5 sample in Fig. 6a. By extracting the off-centering displacement of Nb cations from the Rietveld refinement results in Figs. 5 and 6, the evolution of room-temperature antiferroelectricity in NN ceramics with different grain sizes and poling states can be seen clearly in Figs. 6b-c. Unbalance displacement of Nb1 and Nb2 can be seen for unpoled NN ceramics, which exhibit both

antiferroelectric feature of antiparallel cation displacement and ferroelectric feature of non-zero net polarization (Fig. 6c), thus calling as FiE phase. With decreasing grain size, the displacements of both Nb1 and Nb2 decline monotonously, reflecting as the enhancement of ferroelectricity which was thought to be originated from the increased FE Q phase content before. The critical state for enhancing ferroelectricity should be the formation of FE Q phase like that found in PG5 sample. Along with the increase of ferroelectricity part in the FiE phase, decreased poling strain and remanent strain can be seen during first electric cycle with decreasing grain size, as shown in Fig. S4.

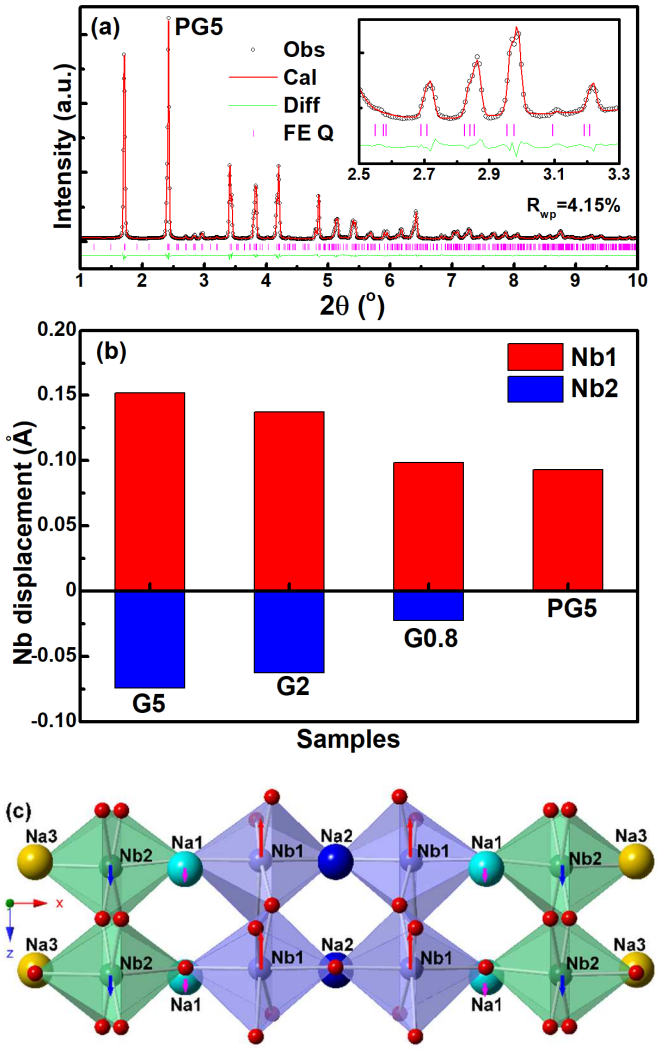

Fig. 6. (a) Rietveld refinement of room-temperature synchrotron XRD (λ=0.1173 Å) results

for PG5 ceramic. (b) Evolution of Nb displacement for various NN ceramics at room temperature. (c) The structure model of FiE $P2_1ma$ phase of NN ceramics.

4.3 Polymorphic phase transition on heating

4.3.1 Polymorphic phase transition in coarse-grain NN ceramic

In order to clarify the origin of polymorphic phase transition behavior of NN ceramics, high-temperature Raman (Fig. 7) and XRD (Figs. 8, 9, S5 and S6) were measured and analyzed. Fig. 7 shows the temperature dependent Raman spectra as well as the deconvolution results of G5 sample. Obvious change of vibration peak number can be found at ~150 ^{o}C and 370 ^{o}C, relating to the two significant dielectric anomalies in Fig. 2a. It is easy to understand the significant change of vibration models caused by the change of polarization configuration and oxygen octahedron tilt features at T_C~370 ^{o}C. There are some different views about the origin of this dielectric anomaly at T_f~150 ^{o}C, which mainly though to be related to the change of ferroelectricity. However, this dielectric anomaly disappears in the poled sample of PG5 with FE Q phase at room temperature (see Fig. 2b), indicating that it should not be related to the FE phase. By looking into the evolution of Raman peaks, the main change around T_f is the mergence of the two peaks around ~75 cm^{-1}, which mainly related to the A-site vibration. The appearance of peak split at room temperature is ascribed to the off-centering displacement of part of Na cations (Na1 in Fig. 6c), which move to the center of oxygen polyhedron during heating across T_f. In other words, the gradual removal of the ferroelectricity originating from Na1 off-centering displacement results in the weak relaxor phase transition at T_f. The phases with (below T_f) and without (above T_f) Na off-centering displacement are marked as P1 and P2, respectively. Along with the change of A-site

vibration during P1-P2 phase transition, the [BO_6] vibration changes slightly without the change of symmetry and polarization configuration features, thus leading to the difficult problem for distinguish P1 and P2 phases from average point of view, which will be discussed in detail by using high-resolution SXRD below.

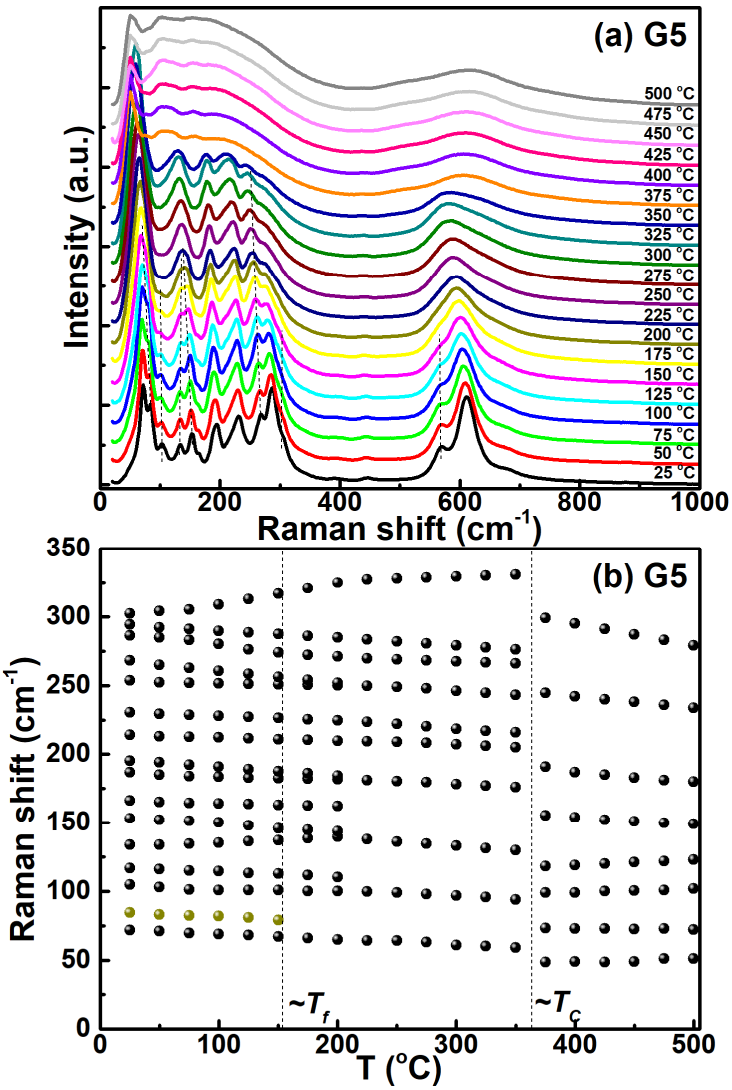

Fig. 7. Temperature dependent (a) Raman spectra and (b) the wave number of several selected Raman peaks by the multiple peak fitting of Gauss-Lorentzian functions for G5 sample.

There is little change of the peak split features for $(3/2\ 1/2\ q)_C$ and $(200)_C$ diffraction peaks on heating till 360 °C, as shown in Fig. 8, suggesting little change of the macroscopic

symmetry and polarization configuration feature caused by Nb displacement and oxygen octahedron tilt. This can be further confirmed by the satisfactory Rietveld refinement result by using the FiE phase in Fig. 9. Owing to the relatively small atomic weight of Na, its displacement information is quite hard to be achieved by XRD results, thus leading to the long-time confusion about the diffuse transition process at T_f.

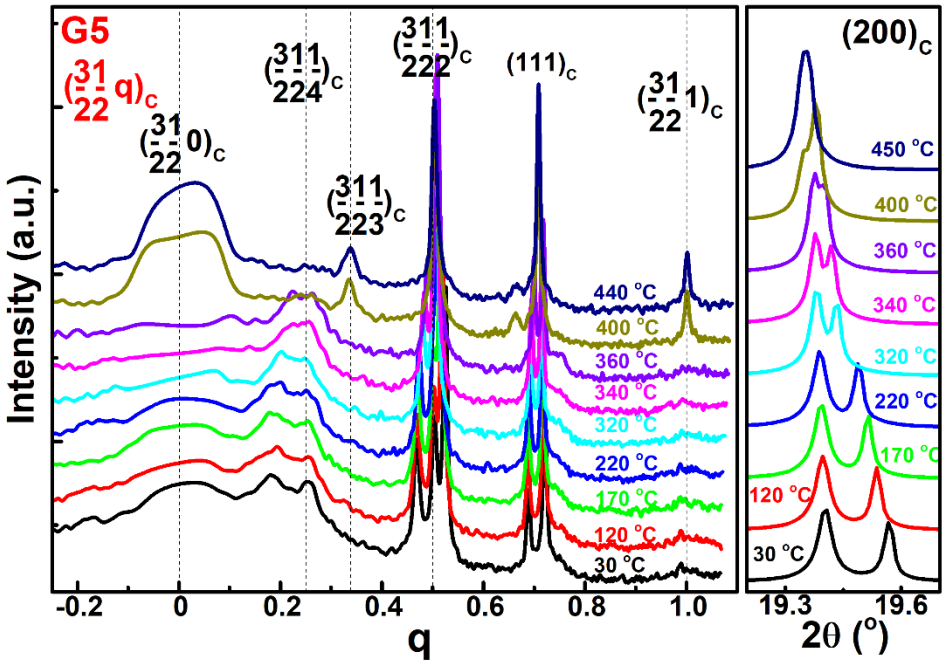

Fig. 8. *(*3/2 1/2 *q)C* and *(*200*)C* diffractions (λ=0.66 Å) for G5 sample at various temperatures.

As heated above 360 °C, the q=1/4 superlattice diffraction peak turns into q=1/3. The previous studies marked the structure in the temperature range of 370~480 °C as AFE R phase, which was identified as an orthorhombic phase with six-fold supercell along c axis. However, the split *(*200*)C* peak as well as weak dielectric anomaly at T_b~410 °C clearly indicates a tetragonal symmetry in the temperature range of 370-410 °C, as shown in Figs. 8 and S5, suggesting a new found AFE tetragonal phase (marked as W phase) in this temperature range. A possible polarization configuration for this new AFE tetragonal phase is supposed and shown in Fig. S7. Owing to the complex cation displacement and oxygen octahedron tilt

information, the detailed structure of this AFE W phase still needs more further studies by using other fine structure analysis technologies in future. The SXRD feature above T_b~410 °C meets the AFE R phase characteristic reported before.

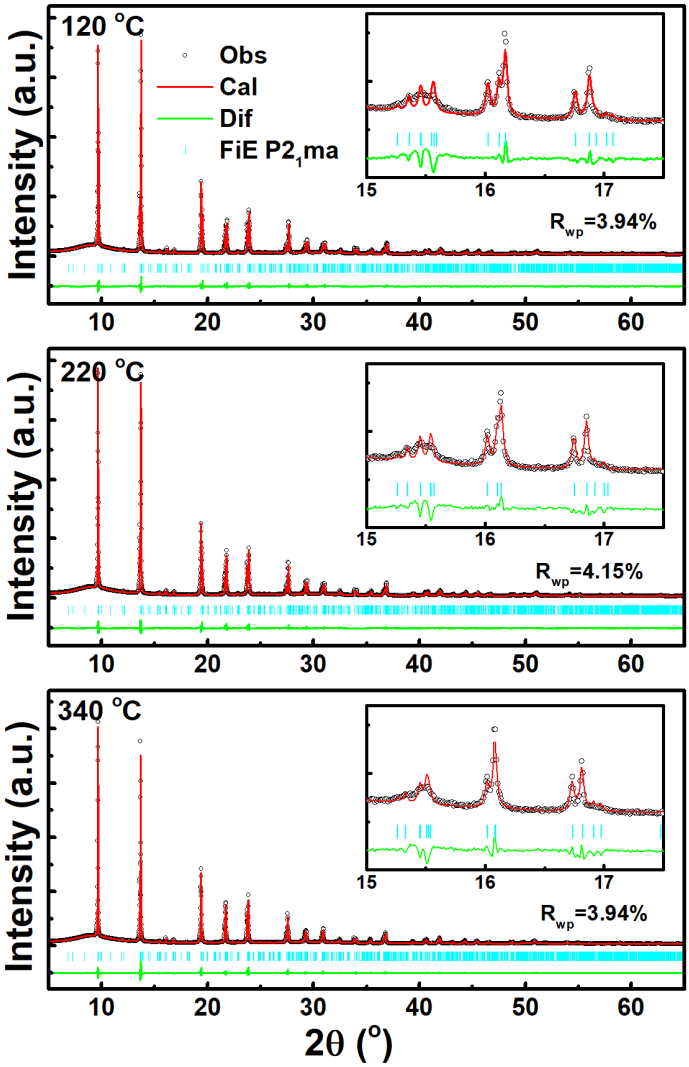

Fig. 9. Rietveld refinement of high-resolution SXRD (λ=0.66 Å) results for G5 ceramic at various temperatures.

4.3.2 Polymorphic phase transition in fine-grain NN ceramic

Besides the change of room-temperature ferroelectricity strength, an additional new phase zone in the temperature range of 320-370 °C can be detected in the NN ceramics with

fine grains (Fig. 2a). High temperature SXRD and XRD for G2 and G0.8 samples was also measured and shown in Figs. 10, 11 and S8-10. Superlattice diffractions (Fig. 10) and the Rietveld refinement (Fig. 11) results indicate the FiE phase can be maintained till 300 °C and then transforms into a tetragonal phase (marked as V phase), which shows q=1/2 and is quite different from the AFE W phase with q=1/3 found above T_C. According to the satisfactory Rietveld refinement results, the structure model of this new found AFE V phase can be given and shown in Fig. S11. Even though there seems to be no phase structure transformation with changing grain size above T_C, obvious change of the lattice parameters can still be found by the change of diffraction peak positions. This indicates that the grain size effect should be originated from the change of interface stress, which changes with changing grain size and exists in all temperature zones. In the studied grain size range, the strength of interface stress can mainly lead to the phase structure transformation of the low temperature phases below T_C but only affects the lattice parameters for the phases above T_C.

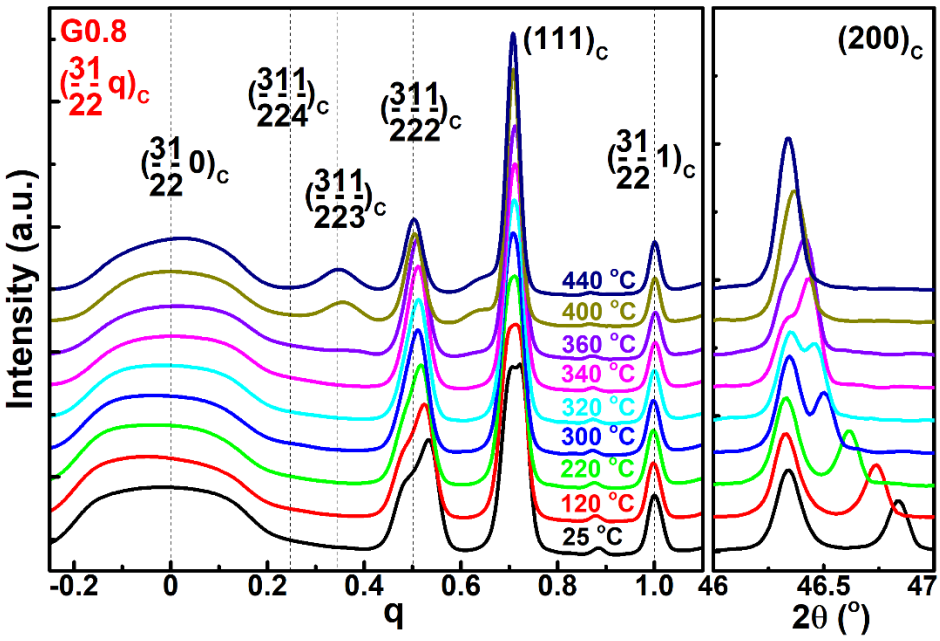

Fig. 10. *(3/2 1/2 q)$_C$* and *(200)$_C$* diffraction peaks for G0.8 sample at various temperatures.

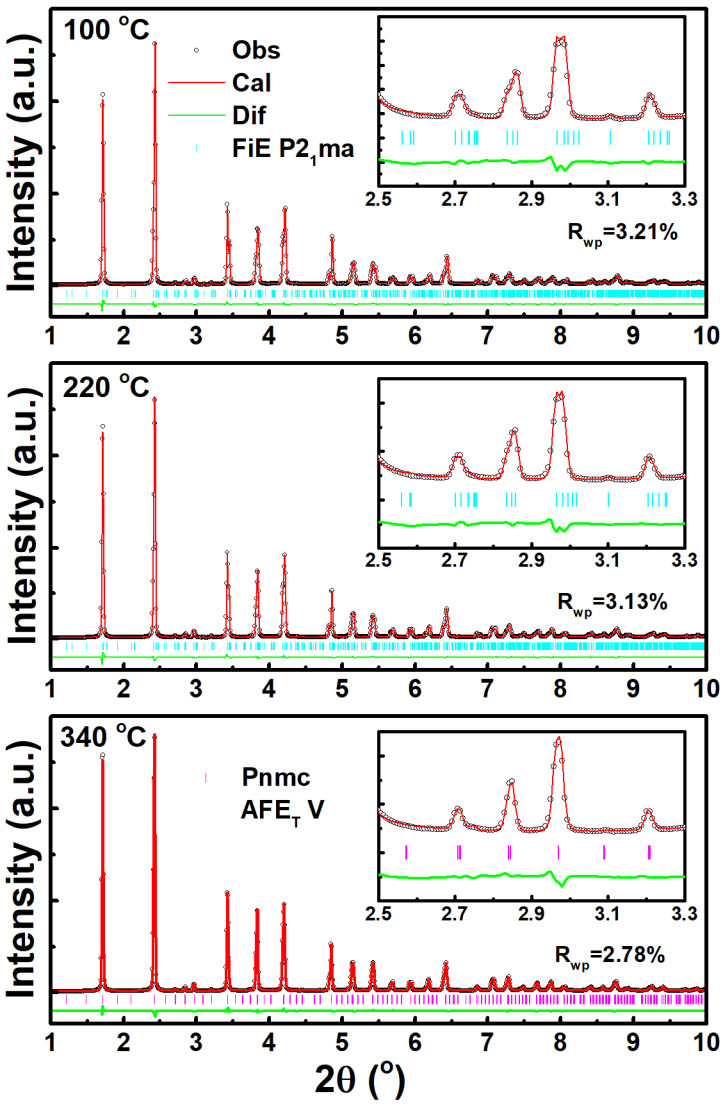

Fig. 11. Rietveld refinement of high-energy SXRD (λ=0.1173 Å) results for G0.8 ceramic at various temperatures

4.3.3 Two-stage depolarization in poled NN ceramic

After poling process at room temperature, FE Q phase with obvious difference of Raman spectra feature can be detected in Fig. 12 for PG5 sample. Owing to the elimination of the Na off-centering displacement during poling, as confirmed by the single Raman peak at ~75 cm^{-1}, the relaxor dielectric peak at T_f disappears in PG5 sample. Along with softening of Nb-O vibrations on heating, the FE Q phase can be detected till ~275 °C, indicating that the AFE-FE

phase transition is irreversible below T_d. Depolarization accompanying with a transformation into AFE phase happens at above T_d, reflecting as obvious change of vibration modes on Raman spectra as well as double *P-E* loops (Fig. 3). However, by comparing the Raman deconvolution results between G5 and PG5 in the temperature ranger of 275-350 ^{o}C, the obvious difference between them indicates that the high-field FE phase does not turn back to the initial FiE phase but transforms into a new AFE phase (marked as Y phase) during discharging process. This incomplete phase transition under electric field has also been reported in NN-based ceramics [32]. Rietveld refinement result of high-energy SXRD suggests that this new field induced AFE Y phase should be monoclinic with *Pm* space group and q=1/2. As heating above T_C, the PG5 sample shows the same structure to the G5 sample, indicating the completion of depolarization process. The completely reversible AFE-FE phase transition has also been reported in NN-based ceramics with AFE R phase [7,32].

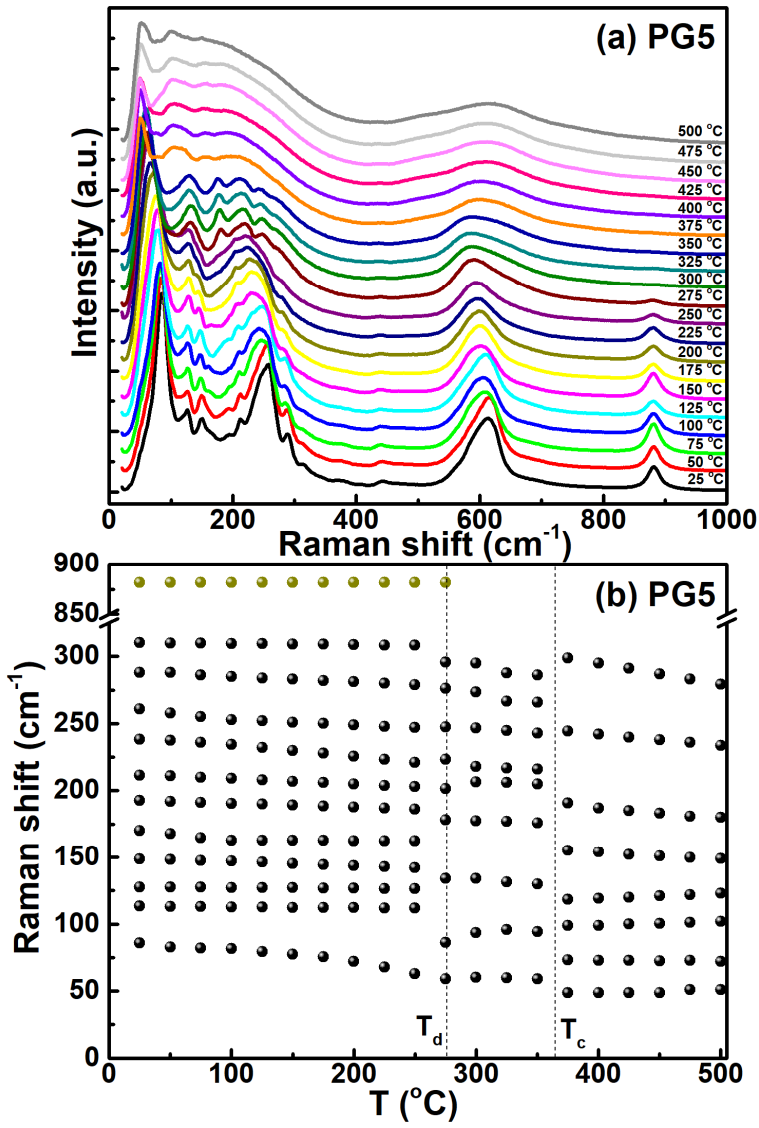

Fig. 12. Temperature dependent (a) Raman spectra and (b) the wave number of several selected Raman peaks by the multiple peak fitting of *Gauss-Lorentzian* functions for PG5 sample.

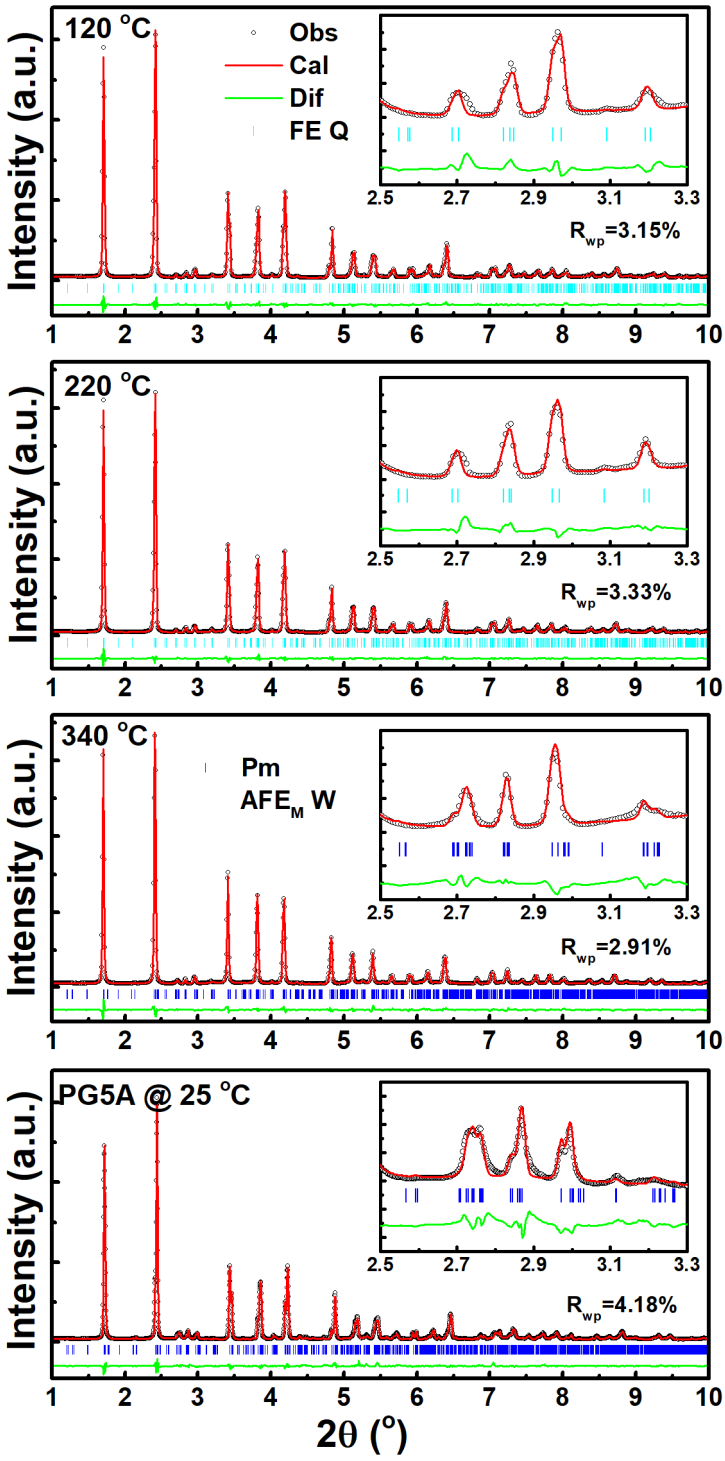

Fig. 13. Rietveld refinement of high-energy SXRD (λ=0.1173 Å) results for PG5 ceramic at various temperatures.

In order to further confirm the two stages of depolarization of the PG5 sample, the electrical properties and phase structure of PG5A (annealed at 320 °C for PG5 ceramic)

sample were studied. The missed dielectric anomaly at T_d suggests that the new AFE W phase can be stabilized to room temperature during cooling. This can be directly confirmed by the Rietveld refinement results shown in Fig. 13. The incomplete depolarization process would also affect the *P-E* and *S-E* characteristics. When the applied electric field on the G5 ceramic is close to E_{AF}, both polarization and strain increase drastically, as shown in Fig. 14. A large poling strain S_{l1}~0.57% can be obtained under 12 kV/mm. After removing of the external electric field, there are a large remanent polarization and a high remanent strain S_{r1}~0.48%. During the application of electric field in the opposite direction, slightly decreased strain can be seen owing to the irreversible non-180^o FE domain switching. As a result, the sample exhibits asymmetric *S-E* curves with a large strain gap of S_{g1}~0.37% on the left side of *S-E* curve on the first cycle. Butterfly shape bipolar *S-E* curve during the second electric field indicates typical FE phase feature of the PG5 sample at room temperature. The asymmetric *P-E* loop shown in Fig. 14c indicates the occurrence of depolarizing on macroscale after annealing at 320 ^{o}C. Even though a drastic increase of strain occurs at around E_{AF}, the poling strain S_{l2} achieved in the PG5A sample is much smaller than that of the G5 ceramic. Large polarization and strain remain when the applied electric field is discharged, indicating the achievement of an FE state. Owing to the irreversible AFE-FE phase transition, asymmetric *S-E* curve with a small strain gap can be seen on the left side of *S-E* curve. The large difference of the poling strain values and strain gap on the *S-E* curves between G5 and PG5A samples confirms an incompletely reversible electric field phase transition at 320 ^{o}C, that is to say, a phase transition from FiE P2 phase to FE phase to AFE V phase during the first electric field cycle at around 320 ^{o}C in NN ceramic.

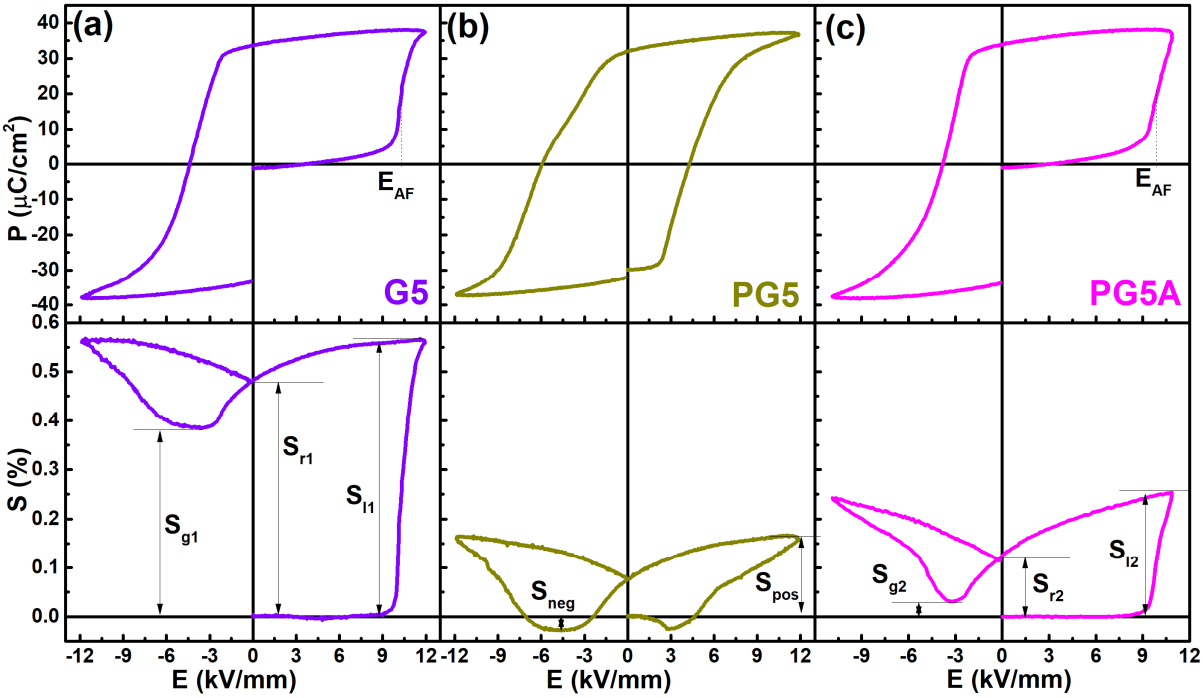

Fig. 14. Room-temperature P-E loops and S-E curves of different NN ceramics.

4.4. Phase diagram

According to the above discussion, a phase diagram, which refers only to an approximation of the long-range structure and may not convey information about the actual structural phase, and lattice parameters evolution of various NN ceramics can be drawn in Fig. 15. Several new insights into the NN ceramics can be given as below:

(1) The room-temperature phase structure of unpoled NN ceramics should be an FiE phase instead of the coexistence of AFE P and FE Q phases. Because there is an obvious difference of free energy between AFE P and FE Q phases slightly below T_C, as confirmed by the repeatable double *P-E* loops, thus the entrance of this phase zone across T_C would not tend to form a coexisted phase. The effect of grain size on ferrielectricity reflects as the change of Nb cations' displacements, which can be supported by the satisfactory Rietveld refinement of high-energy SXRD.

(2) The formation of relaxor dielectric anomaly at T_f~150 ºC should be ascribed to the disappearance of Na1 off-centering displacement without macroscopic symmetry and oxygen octahedron tilt changes, leading to the transition from FiE P1 to FiE P2 phase.

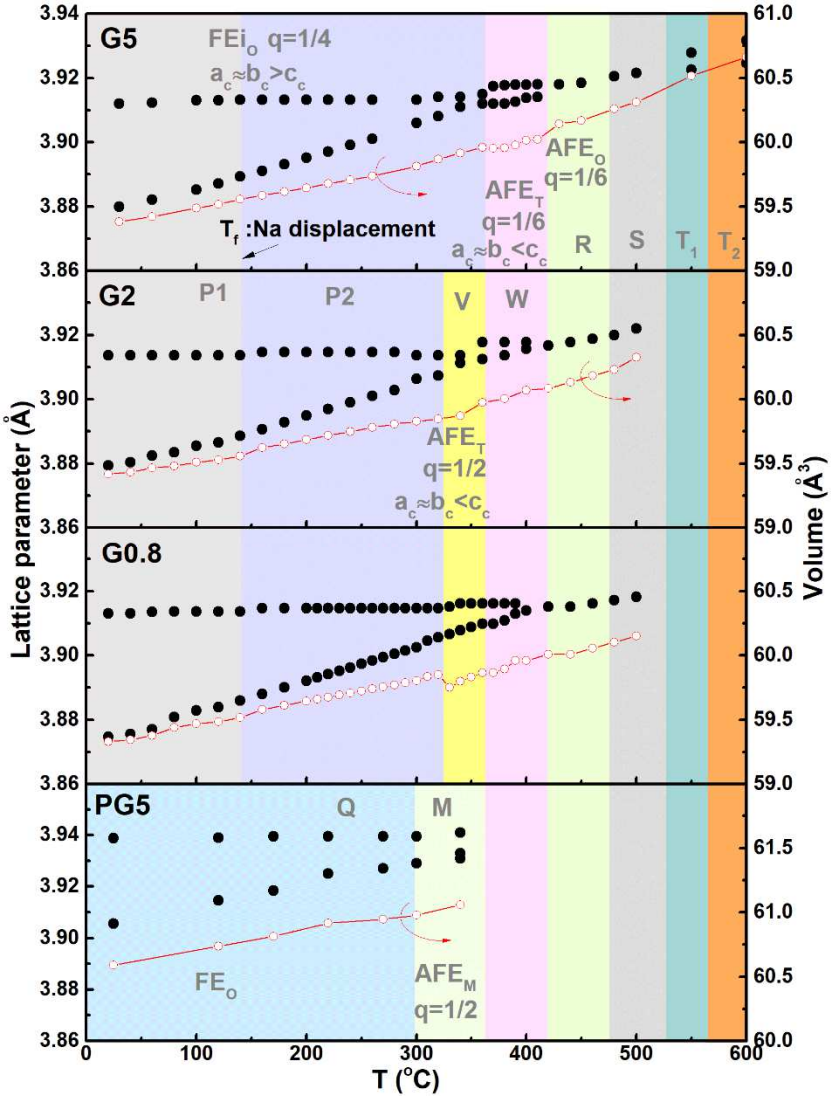

Fig. 15. Average structural phase information evolution of NN ceramics depending on the size effect, poling process and temperature.

(3) The previous proposed AFE R phase zone (370-480 ºC) should include two phase zones: AFE W phase with tetragonal symmetry and q=1/6 in the range of 370-410 ºC and AFE R phase with orthorhombic symmetry and q=1/6 in the range of 410-480 ºC.

(4) With decreasing average grain size to ≤ 2 μm, a new AFE V phase zone with tetragonal symmetry and q=1/2 appears in the temperature range of 320-370 ^{o}C.

(5) The electric field induced phase transition to FE phase gradually changes from irreversible (room temperature to T_d~300 ^{o}C) to incompletely reversible (320-370 ^{o}C, a new AFE V phase appears after discharging) and completely reversible (above T_C~370 ^{o}C). The new found AFE V phase can be maintained to room temperature after annealing in the temperature range of 320-370 ^{o}C for the poled NN sample (namely PG5A sample).

(6) Even though the change of grain size does not lead to the phase transition for the phases above T_C~370 ^{o}C, the changed interface stress can still affect the lattice parameters.

4. Conclusions

Effect of grain size, poling process and heat treatment on the antiferroelectricity of NN ceramic was studied systematically in terms of in-situ SXRD and Raman. The increased grain size would lead to the enhancement of room-temperature antiferroelectricity, while a gradual evolution from irreversible to incompletely reversible to reversible FiE-FE phase transition can be found on heating, thus suggesting that the achievement of double repeatable *P-E* loops in NN-based ceramics should be originated from the shift of high-temperature phase zones to around room temperature. As a result, a new phase diagram based on average structure analysis of NN ceramic was drawn, which would provide a guidance for designing high-performance NN-based AFEs.

Declaration of Competing Interest

The authors declare that they have no known competing financial interests or personal relationships that could have appeared to influence the work reported in this paper.

Acknowledgements

This work was financially supported by the National Natural Science Foundation of China (Grant No. 22235002, 2211101063, 52172181, 22105017) and China Postdoctoral Science Foundation (Grant Nos. 2020M680345 and 2021T140048). This research used resources of the Advanced Pho- ton Source, a U.S. Department of Energy (DOE) Office of Science User Facility operated for the DOE Office of Science by Argonne National Laboratory under Contract No. DE-AC02–06CH11357.

References

[1] E. Sawaguchi, H. Maniwa, S. Hoshino, Antiferroelectric structure of lead zirconate, Phys. Rev. 83 (1951) 1078-1078.

[2] X.L. Tan, C. Ma, J. Frederick, S. Beckman, K.G. Webber, The antiferroelectric ↔ ferroelectric phase transition in lead-containing and lead-free perovskite ceramics, J. Am. Ceram. Soc. 94 (2011) 4091-4107.

[3] X.H. Hao, J.W. Zhai, L.B. Kong, Z.K. Xu, A comprehensive review on the progress of lead zirconate-based antiferroelectric materials, Prog. Mater. Sci. 63 (2014) 1-57.

[4] A.S. Mischenko, Q. Zhang, J.F. Scott, R.W. Whatmore, N.D. Mathur, Giant electrocaloric effect in thin-film $PbZr_{0.95}Ti_{0.05}O_3$, Science 311 (2006) 1270.

[5] W.Y. Pan, C.Q. Dam, Q.M. Zhang, L.E. Cross, Large displacement transducers based on electric field forced phase transitions in the tetragonal $(Pb_{0.97}La_{0.02})(Ti,Zr,Sn)O_3$ family of ceramics, J. Appl. Phys. 66 (1989) 6014-6023.

[6] H. Liu, L. Fan, S. Sun, K. Lin, Y. Ren, X. Tan, X. Xing, J. Chen, Electric-field-induced structure and domain texture evolution in $PbZrO_3$-based antiferroelectric by in-situ high-energy synchrotron X-ray diffraction, Acta Mater. 184 (2020) 41-49.

[7] H. Qi, R. Zuo, A. Xie, A. Tian, J. Fu, Y. Zhang, S. Zhang, Ultrahigh energy-storage density in $NaNbO_3$-based lead-free relaxor antiferroelectric ceramics with nanoscale domains, Adv. Funct. Mater. 29 (2019) 1903877.

[8] A. Chauhan, S. Patel, R. Vaish, C.R. Bowen, Anti-ferroelectric ceramics for high energy density capacitors, Materials 8 (2015) 8009-8031.

[9] B. Gao, H. Liu, Z. Zhou, K. Xu, H. Qi, S. Deng, Y. Ren, J. Sun, H. Huang, J. Chen, An intriguing canting dipole configuration and its evolution under an electric field in La-doped $Pb(Zr,Sn,Ti)O_3$ perovskites, Microstructures 2 (2022) 2022010.

[10] G. Ge, H. Bai, Y. Shi, C. Shi, X. He, J. He, B. Shen, J. Zhai, X. Chou, Optimizing the energy storage properties of antiferroelectric ceramics by modulating the phase structure via constructing a novel binary composite, J. Mater. Chem. A 9 (2021) 11291-11299.

[11] Z. Li, Z. Fu, H. Cai, T. Hu, Z. Yu, Y. Luo, L. Zhang, H. Yao, X. Chen, S. Zhang, G. Wang, X. Dong, F. Xu, Discovery of electric devil's staircase in perovskite antiferroelectric, Sci. Adv. 8 (2022) eabl9088.

[12] G. Ge, C. Shi, C. Chen, Y. Shi, F. Yan, H. Bai, J. Yang, J. Lin, B. Shen, J. Zhai, Tunable domain switching features of incommensurate antiferroelectric ceramics realizing excellent energy storage properties, Adv. Mater. 34 (2022) 2201333.

[13] S.K. Mishra, N. Choudhury, S.L. Chaplot, P.S.R. Krishna, R. Mittal, Competing antiferroelectric and ferroelectric interactions in $NaNbO_3$: Neutron diffraction and theoretical studies, Phys. Rev. B 76 (2007) 024110.

[14] A.C. Sakowski-Cowley, K. Łukaszewicz, H.D. Megaw, The structure of sodium niobate at room temperature, and the problem of reliability in pseudosymmetric structures, Acta Crystallogr., Sect. B: Struct. Crystallogr. Cryst. Chem. 25 (1969) 851-865.

[15] H. Qi, R. Zuo, A. Xie, J. Fu, D. Zhang, Excellent energy-storage properties of $NaNbO_3$-based lead-free antiferroelectric orthorhombic P-phase (Pbma) ceramics with repeatable double polarization-field loops, J. Eur. Ceram. Soc. 39 (2019) 3703-3709.

[16] H. Shimizu, H.Z, Guo, S.E. Reyes-Lillo, Y. Mizuno, K.M. Rabec, C.A. Randall, Lead-free antiferroelectric: $xCaZrO_3$-(1-x)$NaNbO_3$ system ($0 \leq x \leq 0.10$), Dalton Trans. 44 (2015) 10763-10772.

[17] J.M. Ye, G.S. Wang, X.F. Chen, F. Cao, X.L. Dong, Enhanced antiferroelectricity and double hysteresis loop observed in lead-free (1-x)$NaNbO_3$-$xCaSnO_3$ ceramics, Appl. Phys. Lett. 114 (2019) 122901.

[18] L.S. Gao, H.Z. Guo, S.J. Zhang, C.A. Randall, Stabilized antiferroelectricity in $xBiScO_3$-(1-x)$NaNbO_3$ lead-free ceramics with established double hysteresis loops, Appl. Phys. Lett. 112 (2018) 092905.

[19] M.X. Zhou, R.H. Liang, Z.Y. Zhou, S.G. Yan, X.L. Dong, Novel sodium niobate-based

lead-free ceramics as new environment-friendly energy storage materials with high energy density, high power density, and excellent stability, ACS Sustainable Chem. Eng. 6 (2018) 12755-12765.

[20] A. Xie, H. Qi, R. Zuo, A. Tian, J. Chen, S. Zhang, An environmentally-benign $NaNbO_3$-based perovskite antiferroelectric alternative to traditional Pb-based counterparts, J. Mater. Chem. C 7 (2019) 15153-15161.

[21] C.I. Cheon, H.W. Joo, K.-W. Chae, J.S. Kim, S.H. Lee, S. Torii, T. Kamiyama, Monoclinic ferroelectric $NaNbO_3$ at room temperature: Crystal structure solved by using super high resolution neutron powder diffraction, Mater. Lett. 156 (2015) 214-219.

[22] L. Jiang, D.C. Mitchell, W. Dmowski, T. Egami, Local structure of $NaNbO_3$: A neutron scattering study, Phys. Rev. B 88 (2013) 014105.

[23] J. Chen, D. Peng, TEM study of phases and domains in $NaNbO_3$ at room temperature, Phys. Stat. Sol. (A) 109 (1988) 171.

[24] K. E. Johnston, C. C. Tang, J. E. Parker, K. S. Knight, P. Lightfoot, and S. E. Ashbrook, The polar phase of $NaNbO_3$: a combined study by powder diffraction, solid-state NMR, and first-principles calculations, J. Am. Chem. Soc. 132 (2010) 8732-8746.

[25] C. S. Htet, S. Nayak, A. Manjón-Sanz, J. Liu, J. Kong, D. R. Sørensen, F. Marlton, M. R. V. Jørgensen, A. Pramanick, Atomic structural mechanism for ferroelectric-antiferroelectric transformation in perovskite $NaNbO_3$, Phys. Rev. B 105 (2022) 174113.

[26] J.T. Zeng, K.W. Kwok, H.L.W. Chan, Ferroelectric and piezoelectric properties of $Na_{1-x}Ba_xNb_{1-x}Ti_xO_3$ ceramics, J. Am. Ceram. Soc. 89 (2006) 2828-2832.

[27] G. Shirane, E. Sawaguchi, Y. Takagi, Dielectric properties of lead zirconate, Phys. Rev.

84 (1951) 476-481.

[28] J. Koruza, P. Groszewicz, H. Breitzke, G. Buntkowsky, T. Rojac, B. Malič, Grain-size-induced ferroelectricity in $NaNbO_3$, Acta Mater. 126 (2017) 77-85.

[29] Y. Shiratori, A. Magrez, W. Fischer, C. Pithan, R. Waser, Temperature-induced phase transitions in micro-, submicro-, and nanocrystalline $NaNbO_3$, J. Phys. Chem. C 111 (2007) 18493-18502.

[30] B.K. Mani, C.-M. Chang, S. Lisenkov, I. Ponomareva, Critical thickness for antiferroelectricity in $PbZrO_3$, Phys. Rev. Lett. 115 (2015) 097601.

[31] H. Liu, H. Wu, K.P. Ong, T. Yang, P. Yang, P.K. Das, X. Chi, Y. Zhang, C. Diao, W.K.A. Wong, E.P. Chew, Y.F. Chen, C.K.I. Tan, A. Rusydi, M.B.H. Breese, D.J. Singh, L.-Q. Chen, S.J. Pennycook, K. Yao, Giant piezoelectricity in oxide thin films with nanopillar structure, Science 369 (2020) 292-297.

[32] H. Qi, A. Xie, J. Fu, R. Zuo, Emerging antiferroelectric phases with fascinating dielectric, polarization and strain response in $NaNbO_3$-$(Bi_{0.5}Na_{0.5})TiO_3$ lead-free binary system, Acta Mater. 208 (2021) 116710.

[33] A.M. Glazer, The classification of tilted octahedra in perovskites, Acta Cryst. B28 (1972) 3384.

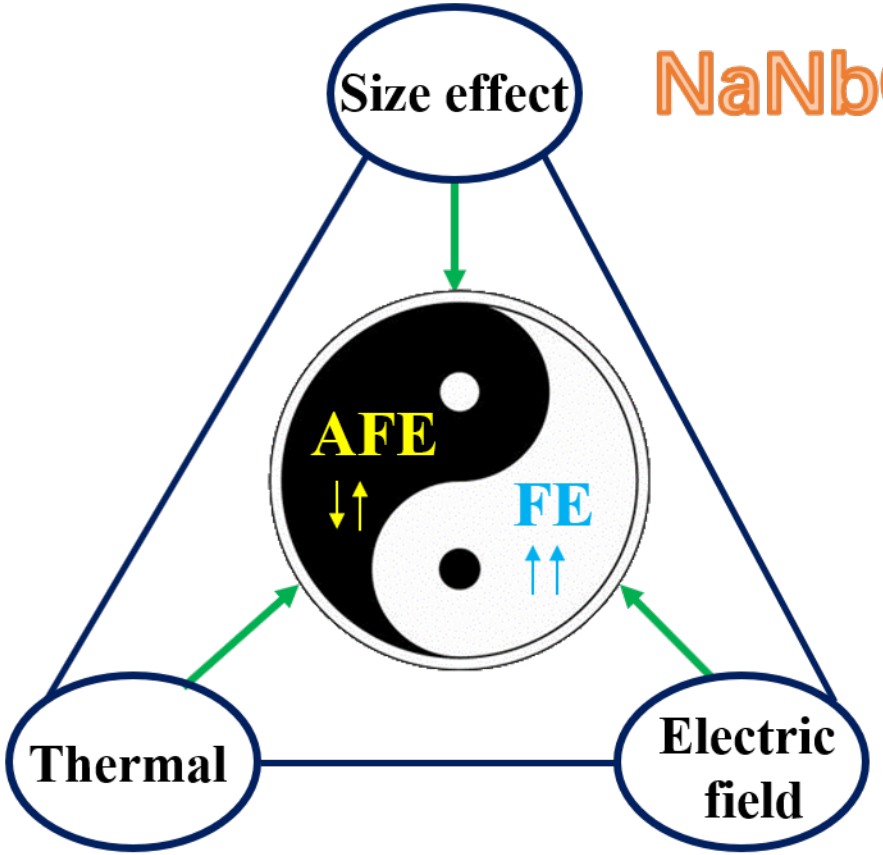
Size effect
NaNbO3
AFE
FE
Thermal
Electric field

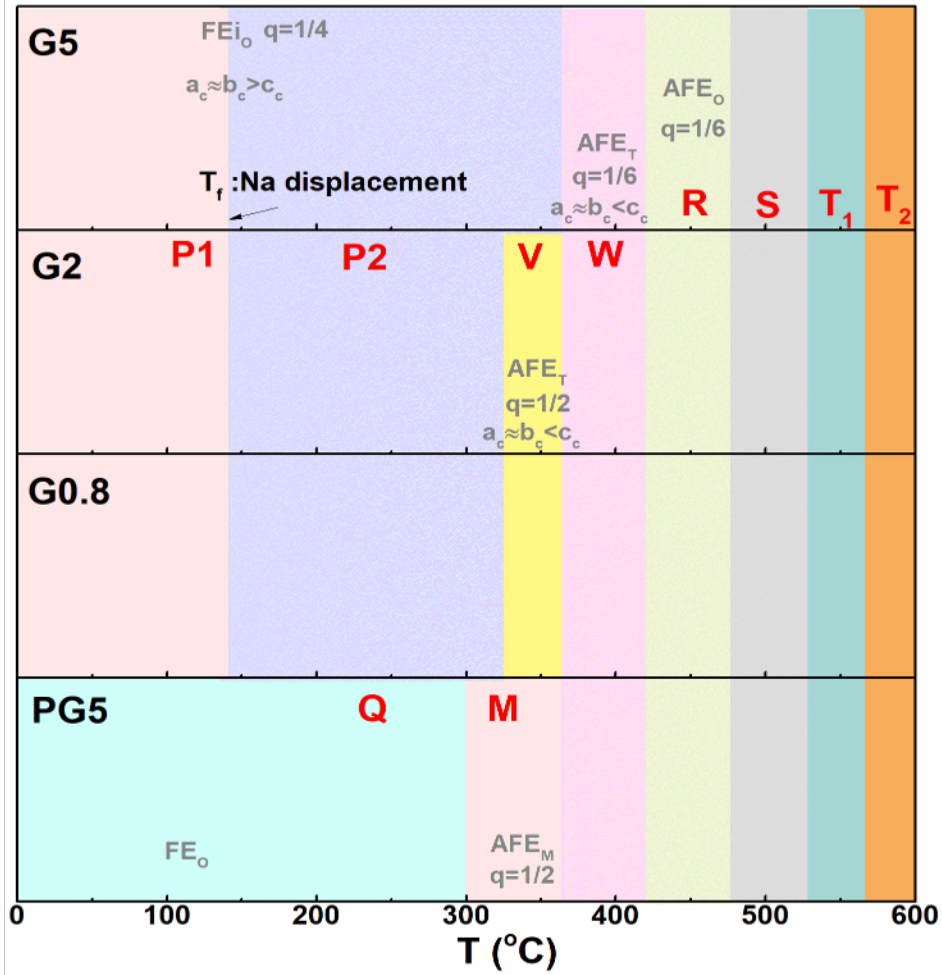
G5
FEi_O q=1/4
a_c≈b_c>c_c
T_f :Na displacement
AFE_T
q=1/6
a_c≈b_c<c_c
AFE_O
q=1/6
R
S
T_1
T_2
G2
P1
P2
V
W
AFE_T
q=1/2
a_c≈b_c<c_c
G0.8
PG5
Q
M
FE_O
AFE_M
q=1/2
0
100
200
300
400
500
600
T (°C)